JOURNAL OF AIRCRAFT
Vol. 48, No. 4, July–August 2011

Steel Structure Impacting onto Water: Coupled Finite Element–Smoothed-Particle-Hydrodynamics Numerical Modeling

A. Grimaldi*
University of Naples "Federico II", 80125 Napoli, Italy
D. J. Benson†
University of California, San Diego, La Jolla, California 92093
and
F. Marulo‡ and M. Guida§
University of Naples "Federico II", 80125 Napoli, Italy

DOI: 10.2514/1.C031258

Ditching in emergency conditions is an important issue for a safe transport plane. Because of the different distributions of loads on the structure, the solutions implemented to secure safety during an impact on the ground are often ineffective in the case of an impact on water. To improve the understanding of the impact dynamics between water and a metallic structure, the Italian Center of Aerospace Research started a preliminary experimental campaign aimed to test the behavior of a simple mockup structure during a water impact. The test specimen was instrumented with accelerometers and pressure sensors linked to a high-speed data acquisition system able to record the time histories to be used for different numerical simulations. Such numerical simulations have been carried out, with different software, both at the DLR, German Aerospace Center and at the Department of Aerospace Engineering at the University of Naples "Federico II". The paper presents the results obtained by using the explicit finite element code LS-DYNA in numerically reproducing each experimental test to define the laws of the materials and correctly simulate the structural behavior under study. The fluid region was modeled using the smoothed-particle-hydrodynamics approach, obtaining a satisfactory numerical–experimental correlation.

I. Introduction

IN CRASH analysis, one of the most important requirements is to assure a survivable aircraft accident. A substantial percentage of aircraft accidents (in particular, rotorcraft accidents) occur on water. Therefore, just as in automobile crashworthiness, it is becoming more and more important to design and build structures that protect the occupants from the impact loads.

The strong interest of the scientific community in the impact of aerospace structures onto water dates back to 1929, when von Kármán carried out a study about the loads encountered during a water impact of a seaplane [1]. Since then, this has been an area of intense research, both experimentally and numerically. Meshless techniques are well suited for solving the issue of mesh where finite element (FE) interpolation encounters difficulties or fails. Mesh-free techniques are often employed locally to overcome the difficulties in the FE calculation, such as remeshing and mesh distortion, etc. Recently, Guida et al. [2] focused their scientific research to model a scenario characterized by large deformations for the impactor as a bird that hit on the aircraft wing leading-edge structure. De Vuyst et al. [3] presented results on the frictionless sliding about the FE–smoothed-particle-hydrodynamics (SPH) coupling, while Chen and Raju [4] studied the numerical method to analyze the phenomenon of a coupled FE and meshless code.

In the last few years, many full-scale drop tests of a fuselage section or rotorcraft were carried out, and they provided a good understanding about fluid–structure phenomena.

For example, Fasanella et al. [5–7] performed many vertical drop tests of an aircraft structure, both on a rigid surface and onto water, providing very important guidelines for the analysis of this type of problem.

The exponential growth in the speed of computers and the even greater decline in the cost of computational resources have been the major contributions to obtaining good results with crash analysis software. In 2003, Randhawa and Lankarani [8] and, recently, Hughes et al. [9] have provided a good assessment of numerical methods to model water impact of rigid aerospace structures and some recommendations for design changes that could potentially improve the offered level of crashworthiness.

This paper reports the results of a project named SPLASH, which had as its main objective the improvement of numerical simulation for analyzing structures impacting on water. The SPLASH project was carried out by collaboration with the Italian Center of Aerospace Research (CIRA), which performed the experimental tests and data acquisition, and the Department of Aerospace Engineering, University of Naples "Federico II", which implemented the numerical analysis of the water impact and its related comparison with the experimental results.

This paper is focused on the numerical aspects of the research, while the experimental results are discussed in [10]. Each numerical simulation has been carried out with LS-DYNA code, and comparison with experimental tests is discussed.

The aim of this paper is to verify the numerical correlation with some experimental measurements of a half-metal stiffened cylinder when impacting the water at different speeds.

The experimental tests were performed at the Italian Laboratory for Impact Tests on Aerospace Structures (LISA) crash test facility located at the CIRA plant. The LISA facility is intended for the study of phenomena of high-energy impact, including (but not limited to) the impacts on the water, and it is able to perform tests on full-scale

Received 6 October 2010; revision received 4 November 2010; accepted for publication 16 November 2010.

*Department of Aerospace Engineering, Via Claudio 21.
†Department of Structural Engineering, 9500 Gilman Drive.
‡Department of Aerospace Engineering, Via Claudio 21.
§Department of Aerospace Engineering, Via Claudio 21; michele.guida@unina.it (Corresponding Author).

structures. It has several unique test facilities and, for the SPLASH project, the drop tower with water impact has been used.

The test article used for the experimental campaign had a simplified geometry that allowed focus on the study of fluid–structure interaction simulations performed by an explicit nonlinear FEM code using the coupled FE–SPH formulation.

II. Numerical Models

A. Finite Element Model of Test Article

The numerical results presented in this paper were obtained by the nonlinear explicit FE code: Livermore Software Technology Corporation's LS-Dyna 971 [11,12]. MSC.Patran [13,14] has been used for the modeling of the test article and water during the preprocessing phase, and LS-PrePost [15,16] was used for the postprocessing of the numerical results. In Fig. 1, the geometry and the FE model (FEM) of the test article is shown; it consists of a half-metal stiffened cylinder with a length of 1200 mm and a diameter of 950 mm. The structure presents three ribs. Two ribs are at the edges of the cylinder and one rib is installed in the middle; each has a hole with a diameter of 150 mm.

The whole structure was modeled; although, in Fig. 1, only the left part is presented for the sake of clarity. The FE consists of three different components: the trolley structure, the cylinder component, and the stiffeners; each of them have been modeled by one-dimensional or two-dimensional elements. The 4200 shell elements used to model the skin of the test article have an average element size of 45 mm. Eighty L-bar and 60 U-bar beam elements were used to model the fixture between the test article and the trolley structure to simulate the stiffeners of the test article. The trolley structure, on which the test article is fixed, is modeled as a rigid plate. An elastic–plastic material law has been used to model the steel in the numerical simulations by defining a piecewise linear curve and Young modulus, a Poisson ratio, a shear modulus, and a plastic stress; while the failure model was based on a maximum plastic strain of 23%. Table 1 shows the material properties of steel used for the manufacturing of the test article and adopted in the numerical model.

All shells in the model are the four-node Belytschko–Tsay element formulation [17], which is based on a combined corotational and velocity-strain formulation [18].

Every analysis was performed on an eight-processor Hewlett Packard Workstation machine with a WIN64 version of LS-Dyna3D (Ver. 971), taking approximately 10 h of elapsed time to complete the first 40 ms of the simulation (i.e., about 80 CPU hours).

B. Water Modeling

The SPH method is a meshless Lagrangian approach developed to study astrophysical problems [19]. The method was also applied to solve computational fluid dynamic problems [20] and, in particular, it was used for continuum mechanics problems with large deformations, such as crash simulations [21].

One difference between the classical FE method and SPH is the methodology of discretization of the model, as shown in Fig. 2. The first figure shows the structure organized in discrete FEs, which defines the FE mesh. The second one defines the SPH discretization in a volume of particles. In the definition of the methodology, a very important role is played by the neighbor search procedure: i.e., the evaluation, step by step, of which particle will interact with the others. This influence of each particle is established inside of a sphere with a radius of $2h$, called the support domain Ωy, where h is the smoothing length, as shown in Fig. 2b.

Table 1 Material properties of the steel test article

Parameter	Value
Density	$\rho = 7850$ kg/m^3
Young's modulus	$E = 2.10 \cdot 10^{11}$ Pa
Tangent modulus	$E_t = 2.00 \cdot 10^9$ Pa
Yield stress	$\sigma_y = 2.35 \cdot 10^8$ Pa
Failure plastic strain	$\epsilon_f = 23\%$

The difference is not just in the discretization but also on the equations. About FE theory, for nonlinear problems, the central difference method is usually adopted, thanks to the stability of the central difference scheme that is determined by looking at the stability of a linear system. The system of linear equations is uncoupled into the modal equations, where the modal matrix of the eigenvectors are normalized with respect to the mass and linear stiffness matrices, K and M, respectively, as reported in [11,22]. The SPH theory is to focus on the conservation equations of mass and energy [19,21,23,24].

In the definition of the SPH formulation, apart from the choice of the number of particles in the model, a very important role is played by the smoothing length h that defines which particle interacts with its neighbors, and it depends on the distribution of particles. The smoothing length of every particle changes with the time [21]. When particles separate (in expansion, for example), a constant smoothing length can lead to numerical fracture, which means that no particle is located in the neighborhood of a given particle; for this reason, the smoothing length increases. When they come close to each other (in compression, for example), a lot of particles will be located in the neighborhood of a given particle, and a smoothing length decreases accordingly.

Another important step of the SPH computation is the neighbor search: i.e., calculating step by step which particle will interact with the others. As shown in Fig. 3, the sphere of the influence of each particle is usually a finite domain of radius $2h$ [21].

The water was modeled by the SPH approach, and it consisted of 66,120 equidistant nodes, where the distance between two nodes was 38 mm, as shown in Fig. 4. The dimensions of the water basin were $1.89 \times 2.4 \times 0.8$ m.

The water was modeled with the material model MAT_NULL (MAT_009) [11,12], which has no shear stiffness, and the Gruneisen equation of state for pressure response.

The Gruneisen equation of state [25] is defined as follows:

$$p = \frac{\rho_0 C^2 \mu\{1 + [1 - (\gamma_0/2)]\mu - (a/2)\mu^2\}}{\{1 - (S_1 - 1)\mu - S_2[\mu^2/(\mu + 1)] - S_3[\mu^3/(\mu + 1)^2]\}} + (\gamma_0 + a\mu)E \tag{1}$$

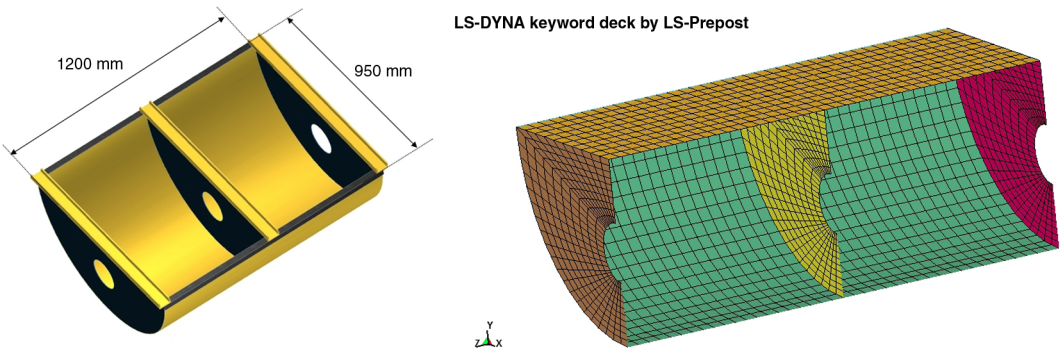

Fig. 1 Geometry and FEM of the test article.

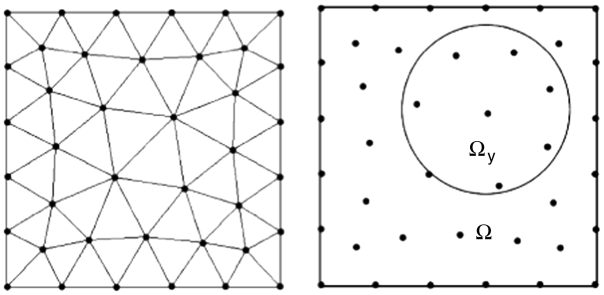

Fig. 2 Discretization of volume: a) FEM and b) SPH.

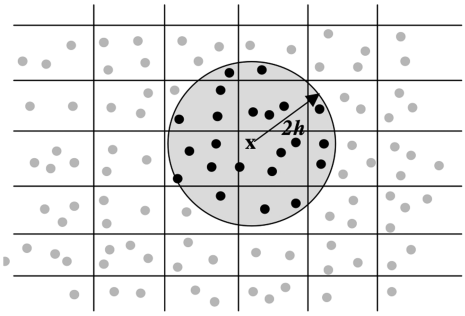

Fig. 3 Domain of the sphere in the SPH method.

where E is the internal energy per initial volume; C is the intercept of the $u_s - u_p$ curve; S_1, S_2, and S_3 are the coefficients of the slope of the $u_s - u_p$ curve; γ_0 is the Gruneisen gamma; and a is the first-order volume correction to γ_0. Constants, C, S_1, S_2, S_3, γ_0, and a are user-defined input parameters. The compression is defined as

$$\mu = \frac{\rho}{\rho_0} - 1 \tag{2}$$

C. Load and Boundary Conditions

To correlate the numerical results with an experimental test conducted by the CIRA, the impact simulation of the test article onto water was performed at three different velocities: 3, 8, and 10 m/s. The test article impacted the water vertically without any significative pitch and roll angles, and gravity had not been taken into account.

To simulate the link between the trolley and the test article, a tied contact was defined between the contact nodes of both parts, which were geometrically in the same position.

Finally, an automatic node-to-surface contact algorithm was used between the shell elements of the test article and the nodes of the water.

The boundary conditions of the water basin have been defined as constraining the nodes of the bottom and lateral surfaces of the block of water. In this way, only the nodes of the upper surface and the interior nodes are free to move in all directions.

III. Numerical Results

Qualitative and quantitative data are analyzed in order to assess global and local correlations between numerical and experimental results. From a qualitative point of view, a numerical simulation has been prepared in order to reproduce the experimental test and to define a fluid–structure interaction between the test article and water. Additionally, for each test case, the numerical simulations are fitted out with numerical global deformations, time histories of the acceleration and skin pressure, and plastic strain distribution in order to evaluate the behavior of the test article as a result of the impact.

The quantitative numerical–experimental correlation has been performed collecting some time histories of the accelerations and pressures of the test article during the different impacts.

The accelerations of the numerical model were retrieved at four nodes of the FE mesh corresponding to the positions of accelerometers used in the experimental test, as shown in Fig. 5.

Analogously, the pressures were measured at the seven nodes corresponding to the positions of the pressure transducers used during the experimental tests, as shown in Fig. 6. The pressure at a node is calculated as its resultant force divided by one-quarter of the area of the shell elements attached to it. The origin of the reference is defined in the center of the rib hole. Because of symmetry, only the pressure time histories of a quarter of the numerical test article are shown and the unfiltered numerical data Eulerian formulation with CFC180 filtered [26] numerical data.

Finally, to obtain a measurement of permanent deformations in the structure, as in the experimental test [10], a map with measurement points was defined, resulting in seven sections on the skin, from A to G (Fig. 7), and nine nodes for each section to measure the relative displacement of the skin before and after the impact.

A. Impact Velocity 3 m/s

According to the test scenario, three analyses at 3, 8, and 10 m/s have been computed. Figure 8a shows the interaction between the test article and water in the case of impact at the velocity of 3 m/s at the end of the simulation time ($t = 40$ ms).

Figure 8b shows the plot of the effective plastic strains of the test article at the end of the impact, with no significant deformations, and a maximum effective plastic strain ϵ_p equal to 0.2007%.

Figure 9 shows the time history of accelerometer A1 obtained from the simulation at 3 m/s, comparing the unfiltered curve with one filtered by a digital filter based on the Society of Automotive Engineers CFC60 (channel frequency class) specifications [26]. The four numerical acceleration time histories always have the same behavior, and in the following sections, the time history of the A1 accelerometer is reported.

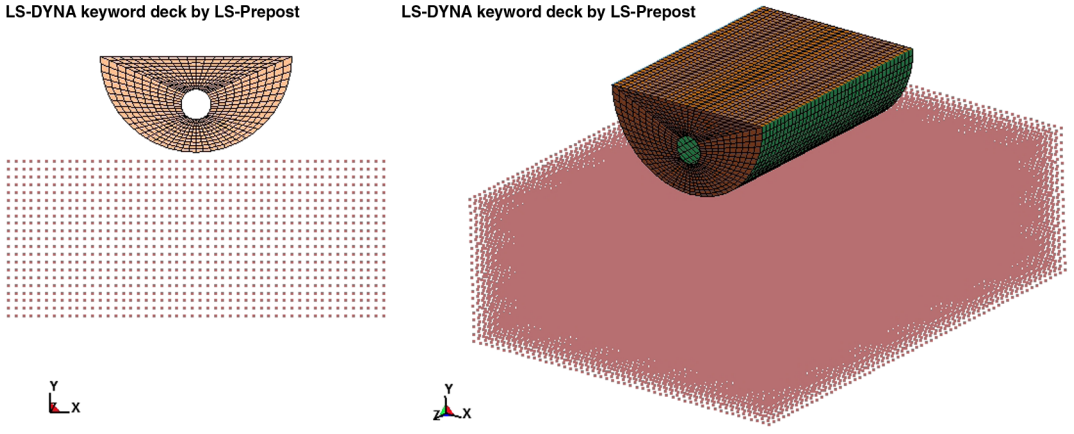

Fig. 4 SPH model of the water.

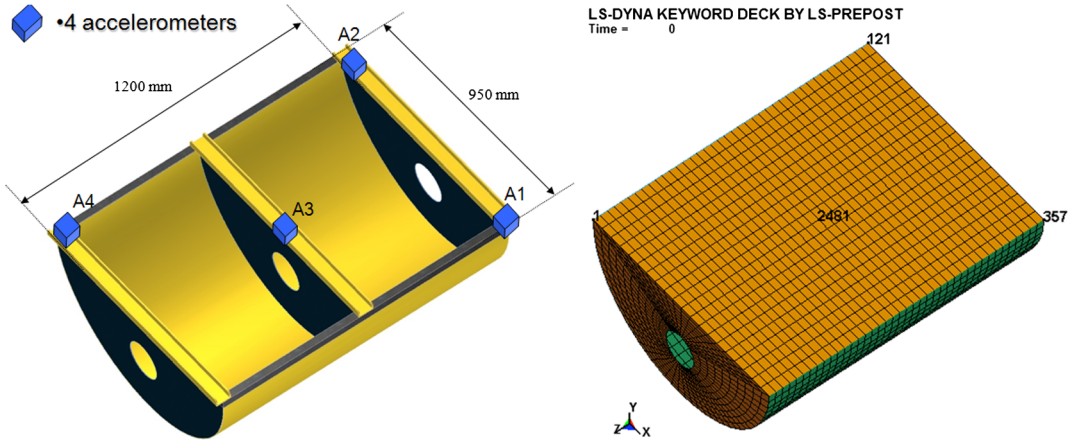

Fig. 5 Accelerometer positions and FE corresponding nodes.

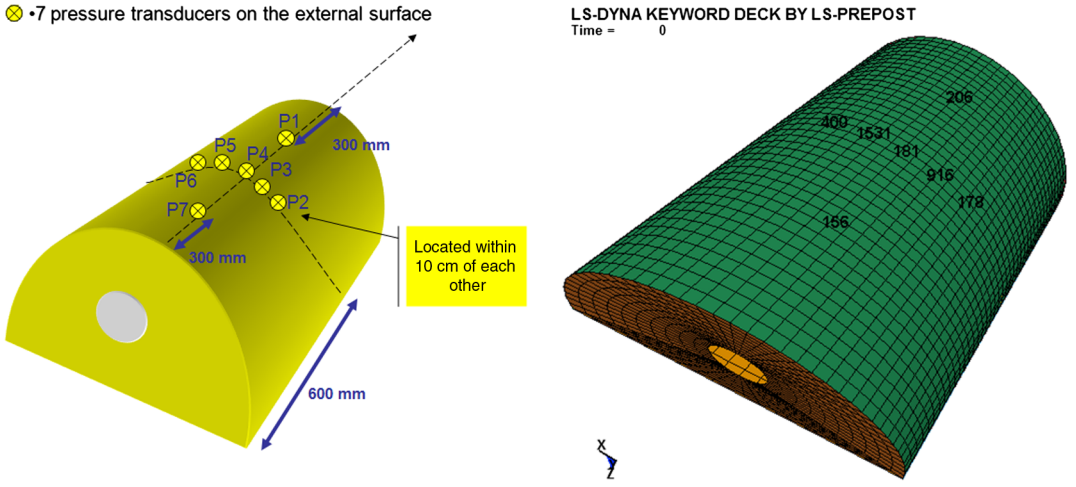

Fig. 6 Pressure transducer positions and FE corresponding nodes.

Figures 10a and 10b show, respectively, the time histories of the pressure under the central frame of the structure (P4) and between two frames (P1).

B. Impact Velocity 8 m/s

Figure 11a shows the interaction between the test article and water in the case of impact at a velocity of 8 m/s. The phenomenon of water sloshing during impact is clearly shown, which is well represented by the SPH approach. SPH appears to be robust and accurate for analysis of this kind of fluid phenomenon compared with other approaches, like the Lagrangian [27,28], the Eulerian, or the arbitrary Lagrangian Eulerian formulation [29].

Figure 11b shows the plot of the effective plastic strains ϵ_p of the test article at the end of the impact phenomenon, with a maximum ϵ_p equal to 0.02045%.

Again, Fig. 12 shows the time history of the accelerometer A1 obtained from the numerical simulation and the comparison between the unfiltered curve with the CFC60 filtered one.

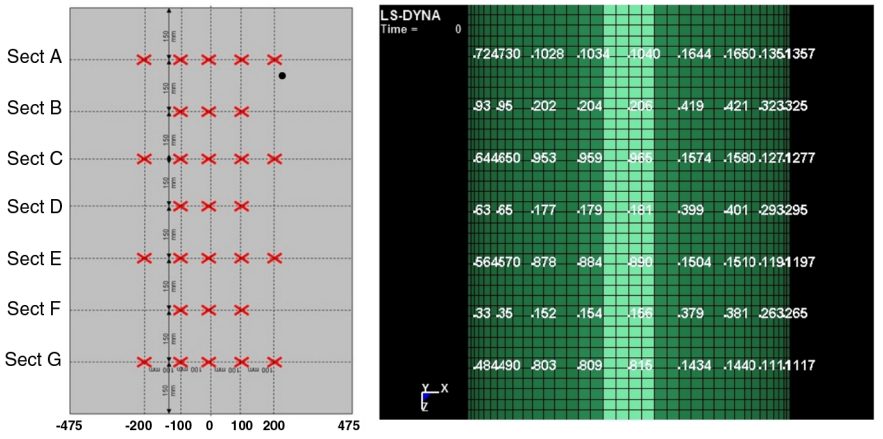

Fig. 7 Sections of the skin for the calculation of relative displacement.

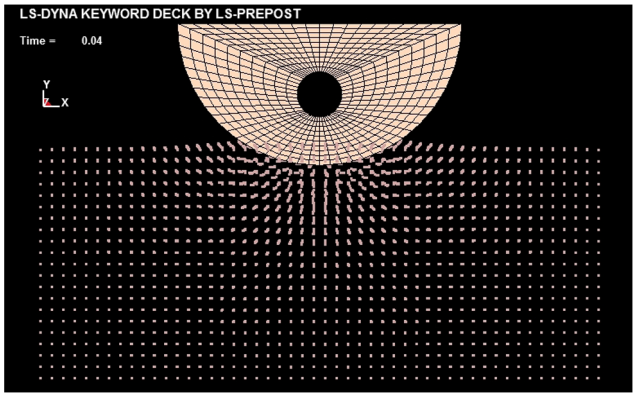

a) Structure and water interaction at 3 m/s

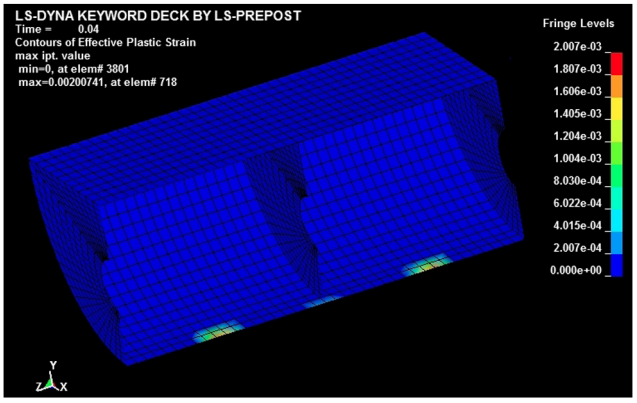

b) Effective plastic strain of the skin at 3 m/s

Fig. 8 Global behavior of the test article.

The following Figs. 13a and 13b analogously show the time histories of the pressure under the center frame (P4) and between two frames (P1).

Unlike the case of the simulation at 3 m/s, after the impact at 8 m/s, as shown in Fig. 14a, there are significant deformations of the skin. In Fig. 14b. the relative displacement of Sec. III.B, located at the center of two frames, has a maximum deformation of 35 mm. This numerical value, compared with the experimental value measured on the test article in the condition of the postimpact test, has a negligible error of less than 5%.

C. Impact Velocity 10 m/s

A list of results is presented for the case of the 10 m/s impact velocity. Figures 15a and 15b show, respectively, the global interaction between the structure and the water and the behavior of the maximum effective plastic strain that, in this particular case, reaches the value of 0.03002.

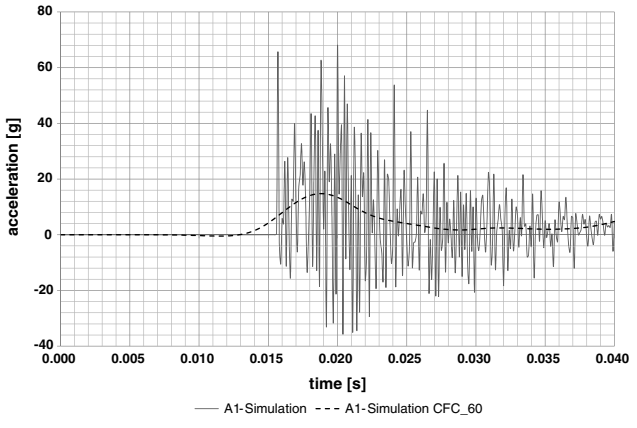

Fig. 9 Time history of accelerometer A1 at 3 m/s.

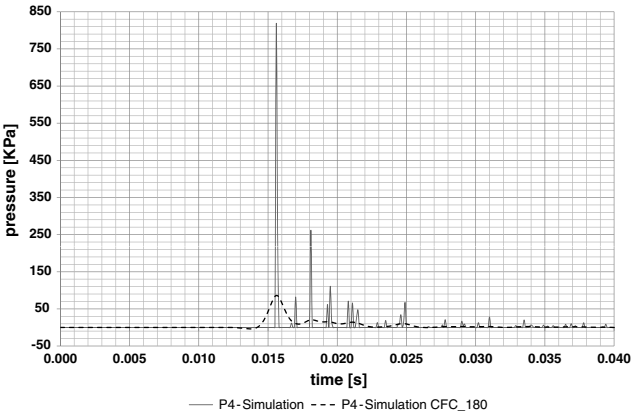

a) Pressure under the center frame (P4)

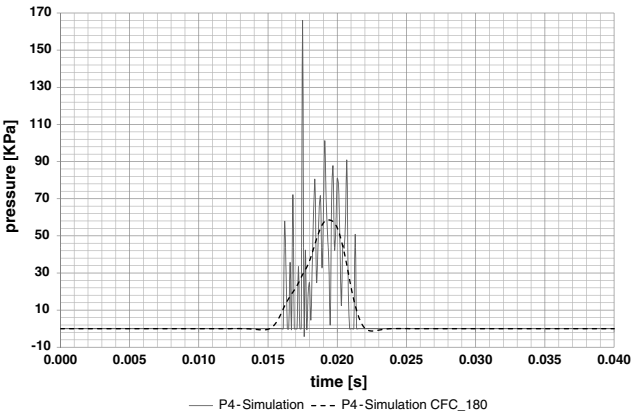

b) Pressure under the skin between two frames (P1)

Fig. 10 Time histories of the pressure at 3 m/s.

Figure 16 shows the time history of accelerometer A1 obtained in the simulation at 10 m/s and the comparison between the unfiltered curve with the CFC60 filtered one.

The comparison of the CFC180 filtered and unfiltered results for the same positions of the previous cases is reported in Fig. 16 for the

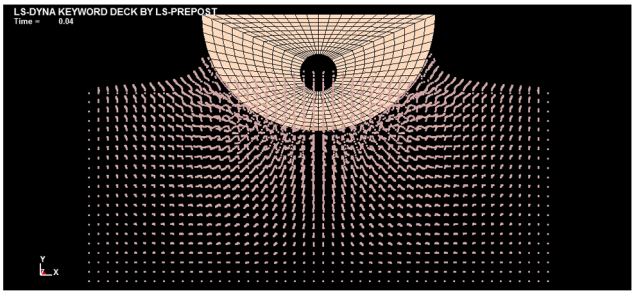

a) Structure and water interaction at 8 m/s

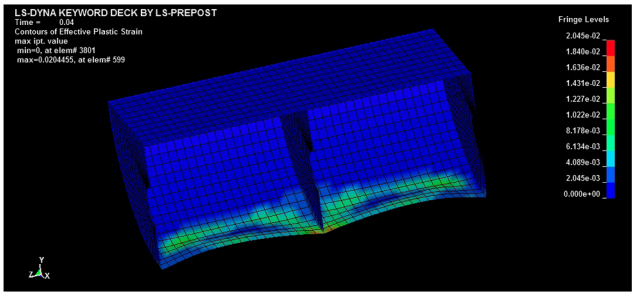

b) Effective plastic strain of the skin at 8 m/s

Fig. 11 Global behavior of the test article at 8 m/s.

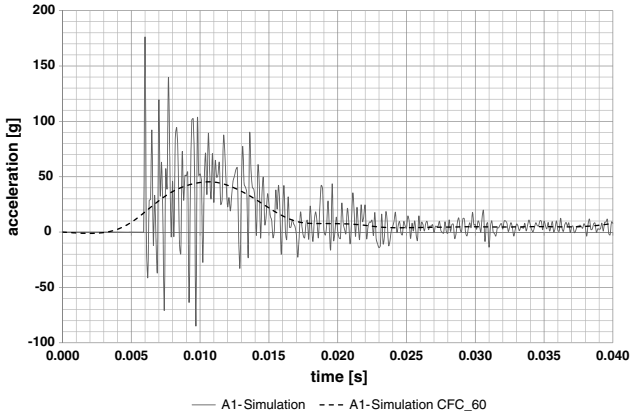

Fig. 12 Time history of accelerometer A1 at 8 m/s.

acceleration and in Figs. 17a and 17b for the pressures at the two different locations.

As expected, noticeable deformation has occurred, as shown in Fig. 18a, with a maximum relative displacement equal to 50 mm, measured in section B of the skin between the two frames; see Fig. 18b. This numerical value compared with the experimental value, measured on the test article in the condition of the postimpact test, has a negligible error of less than 5%. Almost symmetrical deformation is evidenced by Fig. 18a, which is in agreement with the experimental results.

IV. Numerical and Experimental Correlation

The last part of this research is focused on the correlation between the numerical results, obtained with LS-Dyna, and the experimental results, obtained by the test campaign performed in the CIRA facility.

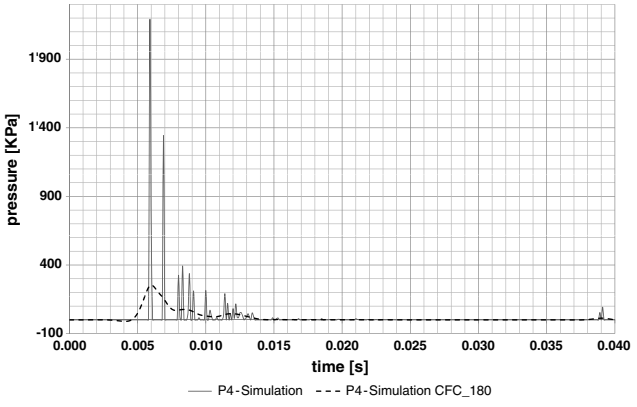

a) Pressure under the center frame (P4)

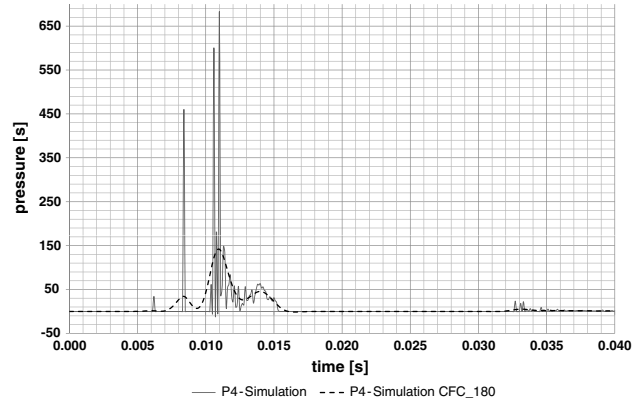

b) Pressure under the skin between two frames (P1)

Fig. 13 Time histories of the pressure at 8 m/s.

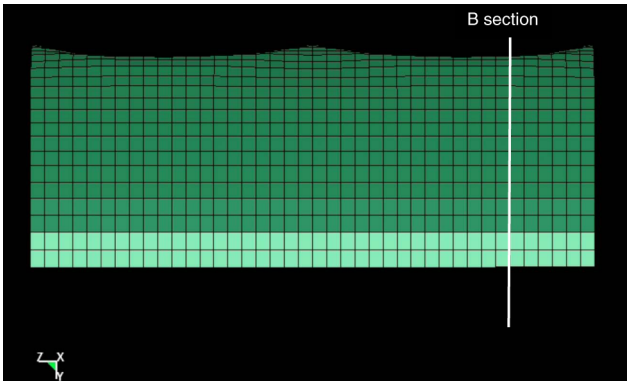

a) Shape of the skin after the impact

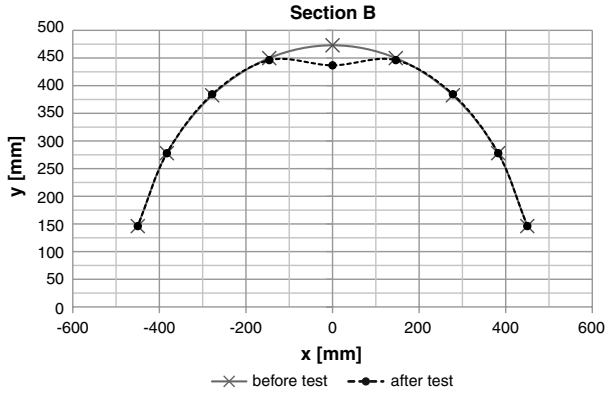

b) Measurement of deformation of B section between two frames

Fig. 14 Skin deformation at 8 m/s.

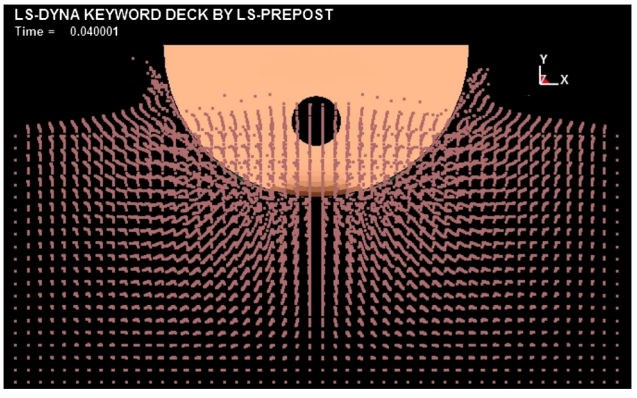

a) Structure and water interaction at 10 m/s

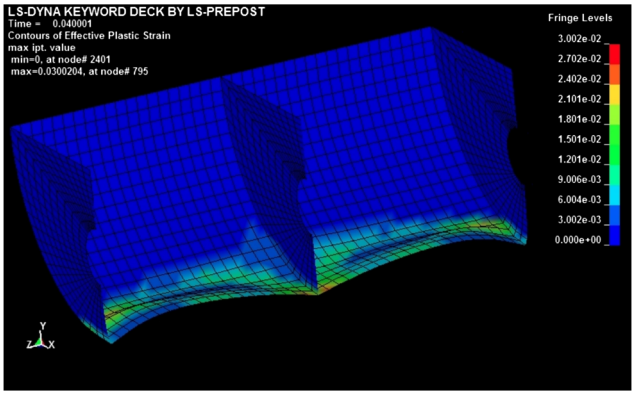

b) Effective plastic strain of the skin at 10 m/s

Fig. 15 Global behavior of the test article at 10 m/s.

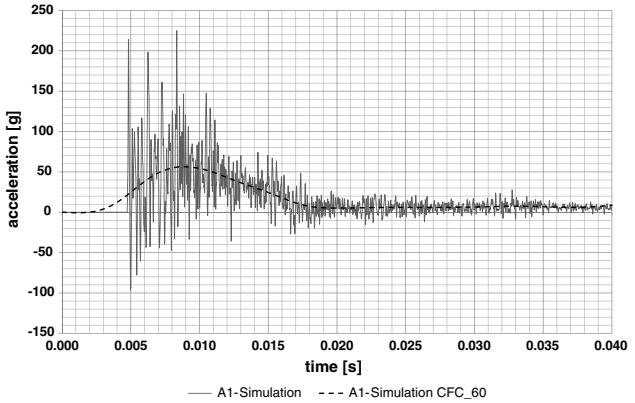

Fig. 16 Time history of accelerometer A1 at 10 m/s.

The first stage of correlation concerns the behavior of the numerical and experimental time histories of the pressure and acceleration and an evaluation of the global deformation of the structure to assure that the simulation, performed by the explicit FE code, is able to represent and reproduce the impact phenomenon of the structure onto water.

The second stage of the numerical–experimental analysis is the comparison between the peak values of accelerations, pressures, and deformations calculated by the numerical analysis and measured by experimental tests.

A. Acceleration Time Histories

Figure 19 shows the comparisons between the numerical and experimental acceleration time histories. It shows a quite satisfactory agreement between the predicted and measured data in terms of the overall shape of the curve and its peak curve, which is slightly overestimated. The three time histories of the acceleration, each refers to three drop heights, present an initial peak and then different damped oscillations with lower amplitudes, which depend on oscillation of the test article as soon as it impacts on the water. The simulated maximum acceleration levels for each impact differ by 20% (impact at 3 m/s), 13% (at 8 m/s), and 18% (at 10 m/s) from the experimental recorded accelerations (12, 40, and 46 g). The shape and pulse length are in good agreement, whereas because of the low weight of the test article, even minor ripples in the free surface can significantly change the measurements of deceleration and deformation. For this reason, it was necessary to perform a greater number of tests (at the same drop height) to ensure repeatability and accuracy in the acquired data.

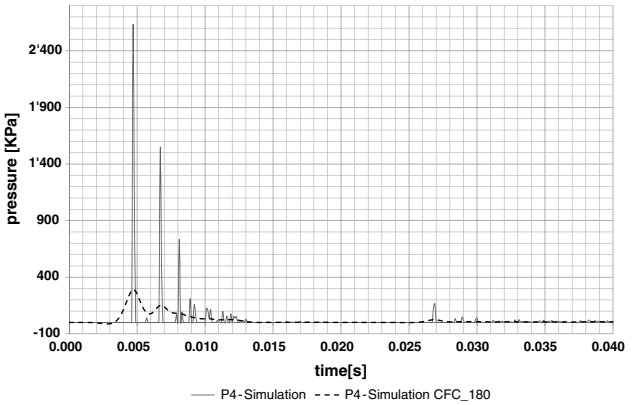

a) Pressure under the center frame (P4)

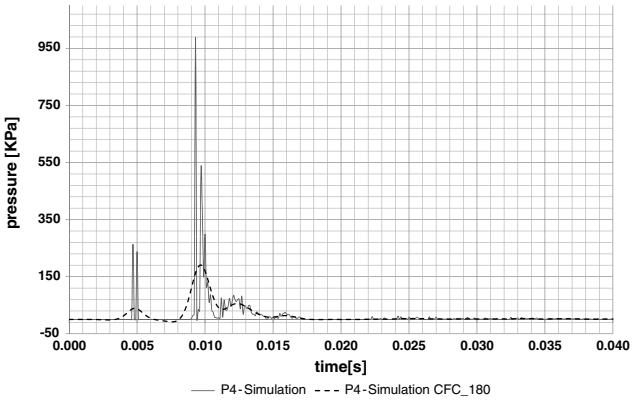

b) Pressure under the skin between two frames (P1)

Fig. 17 Time histories of the pressure at 10 m/s.

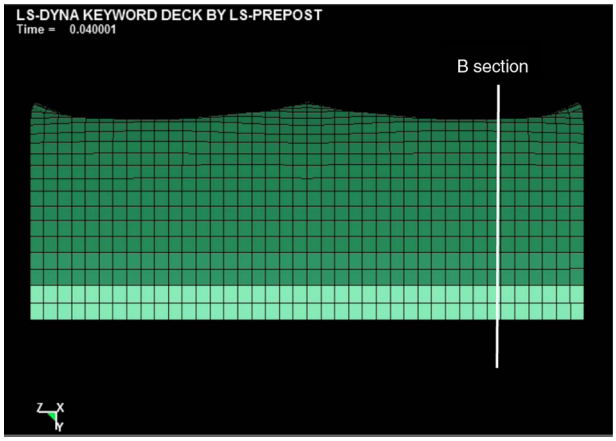

a) Shape of the skin after the impact

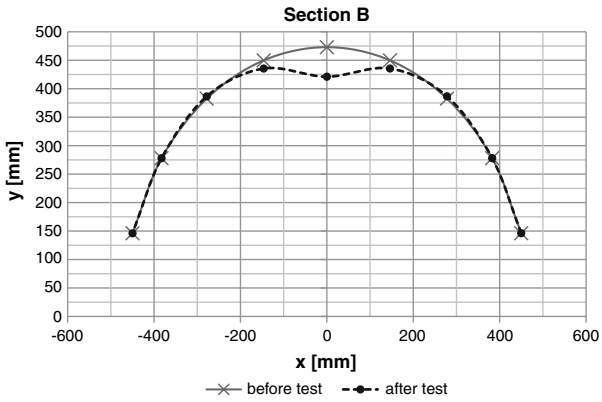

b) Measurement of deformation of B section between two frames

Fig. 18 Skin deformation at 10 m/s.

B. Pressure Time Histories

As can be seen from Figs. 20 and 21, the simulation overestimates the experimental time history of the pressure related to position P4 under the center frame of the structure, whereas it underestimates the pressure measured in position P1 under the structure between two frames. For both locations, however, the time behavior results in a more rapid change for the experimental results than the numerical simulations.

Correlating the time histories of the accelerometers with pressures, it is possible to evaluate that the accelerometers furnished a global measurement that illustrates the whole period of the first contact phase, while the pressures give the local measurements that are generated by pressure fluctuations. Mesh density studies suggested a mesh of 1 mm, both the breadth and length dimensions were sufficient to capture the impact; this enables visualization of the waves

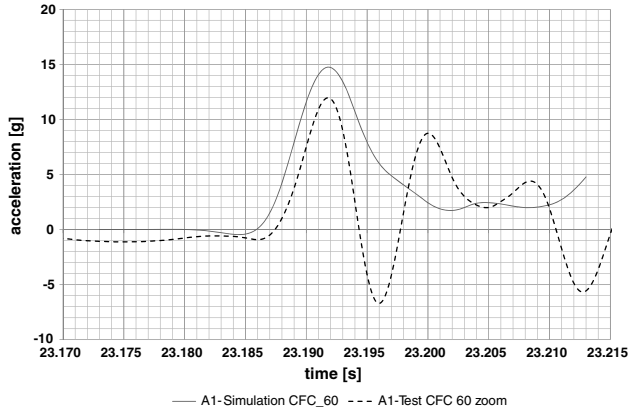

a) Impact at 3 m/s

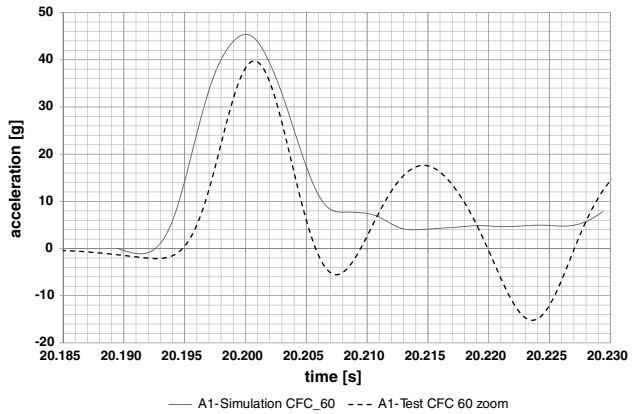

b) Impact at 8 m/s

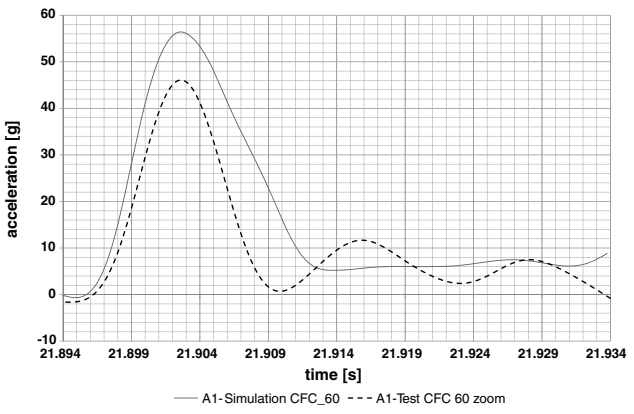

c) Impact at 10 m/s

Fig. 19 Acceleration time histories comparison.

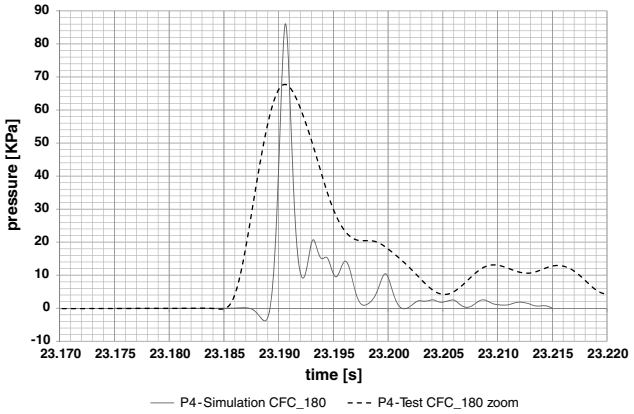

a) Impact at 3 m/s

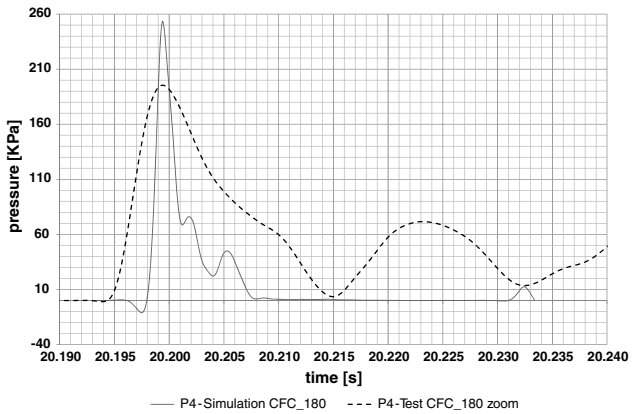

b) Impact at 8 m/s

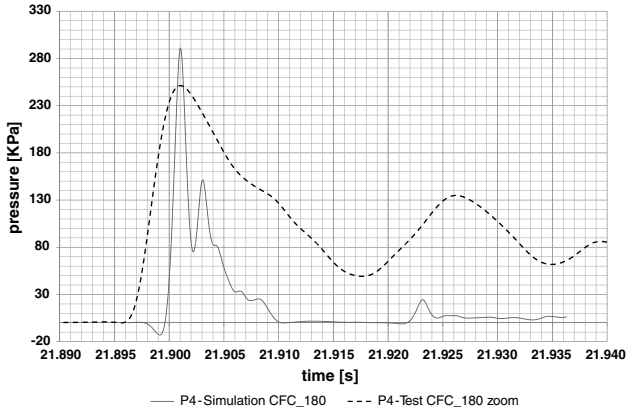

c) Impact at 10 m/s

Fig. 20 Pressure time histories comparison under the center frame (P4).

generated by the impact. The resulting pressure profiles in the plates are shown for a time of 5 ms. At 5 ms, the plates are in contact and the stress wave will shortly reach the free ends.

V. Results

The global behavior of the experimental tests has been fully reproduced with satisfactory approximation and coherent trend comparison. On the other hand, the numerical comparisons of single values show that the error percentages are not negligible, as shown in Table 2, where a summary of the peak values in terms of accelerations and pressures is presented.

The differences between the numerical and the experimental values presented in Table 2 should not be considered as a lack of confidence in the model. The effort of the analyst is generally not directed to the exact reproduction of each single value obtained during the test but to its order of magnitude. Much more interest should be dedicated to the global behavior of the structure, with this result being much more interesting from engineering and design points of view.

The results of the research emphasize three main issues:

1) The acceleration is the parameter that better correlates with the experimental data, and it is also the most robust result to be selected from the measurement.

2) The correlation between numerical and experimental results has shown the limited accuracy of the pressure prediction, which is a sensitive parameter to calculation and measurement during the impact.

3) The SPH approach appears to be a very effective formulation for the modeling and global reproduction of the water impact phenomenon.

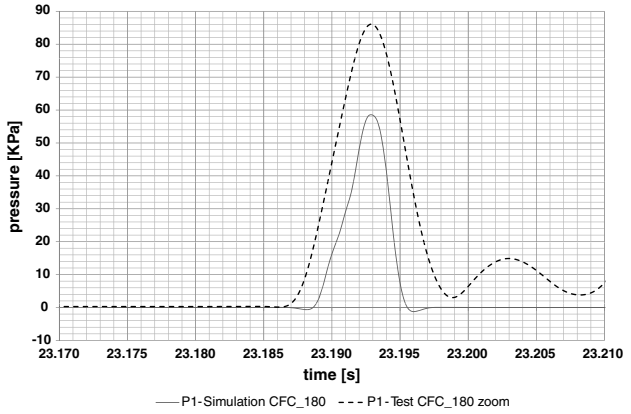

a) Impact at 3 m/s

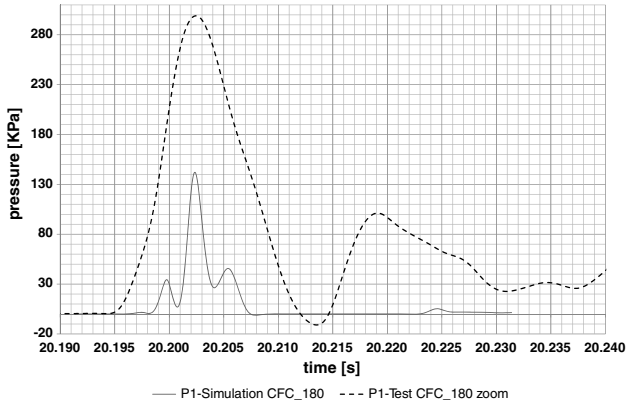

b) Impact at 8 m/s

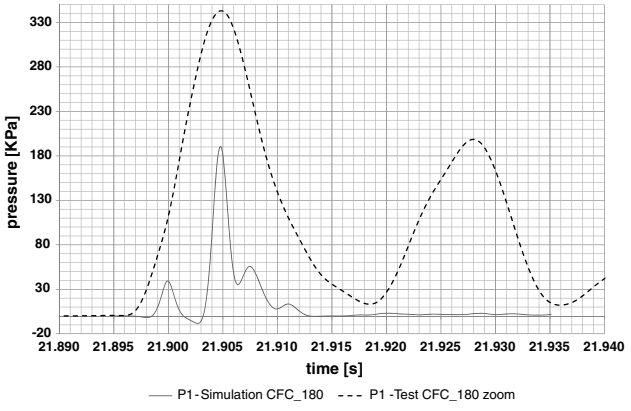

c) Impact at 10 m/s

Fig. 21 Pressure time histories comparison under the skin between two frames (P1).

VI. Conclusions

The paper has described a campaign of numerical simulations using the nonlinear explicit software LS-Dyna conducted on a steel structure impacting on water at 3, 8, and 10 m/s.

The goal of the work was to estimate the efficiency of the nonlinear explicit software to predict the response of a metallic structure subjected to water impact, and it was part of a more complex research project aimed to improve the knowledge of the water impact of metallic structures. The main interest of the numerical simulations has been the modeling of the water passing through different formulations, of which only the SPH approach has been herein reported.

As result of an impact that, in most cases, is a destructive event, the main interest is the understanding of how the energy involved is absorbed by the structure and how a proper structural design may optimize each structural component to deform in a manner that minimizes the amount of impacting energy transferred to the occupants.

Such a result, which may be referred to as a global behavior of the impacting structure, is fully and very satisfactorily reproduced by the numerical model; therefore, such simulations should be considered well worth their extensive numerical effort.

Acknowledgments

The present work belongs to the SPLASH project (Assessment of Methods and Modelling Rules for Numerical Simulation of Ditching Phenomena), supported by the Campania Regional Government. Precious insights about the specific topics were gained by collaboration with the Department of Structural Engineering, University of California, San Diego, where the first author spent months (from March to September 2009) as a visiting scholar under the supervision of David J. Benson. That visit was partially supported by a grant received from the University of Naples "Federico II" through the Ufficio Dottorato, Assegni e Borse di Studio and the Department of Aerospace Engineering of the same university.

References

[1] von Kármán, T., "The Impact of Seaplane Floats During Landing," NACA TN 321, 1929.

[2] Guida, M., Marulo, F., Meo, M., Grimaldi, A., and Olivares, G., "SPH-Lagrangian Study of Bird Impact on Leading Edge Wing," *Composite Structures*, Vol. 93, No. 3, 2011, pp. 1060–1071. doi:10.1016/j.compstruct.2010.10.001

[3] De Vuyst, T., Vignjevic, R., and Campbell, J. C., "Coupling Between Meshless and Finite Element Methods," *International Journal of Impact Engineering*, Vol. 31, No. 8, 2005, pp. 1054–1064. doi:10.1016/j.ijimpeng.2004.04.017

[4] Chen, T., and Raju, I. S., "A Coupled Finite Element and Meshless Local Petrovâgalerkin Method for Two-Dimensional Potential Problems," *Computer Methods in Applied Mechanics and Engineering*, Vol. 192, Nos. 41–42, 2003, pp. 4533–4550. doi:10.1016/S0045-7825(03)00421-3

[5] Fasanella, E. L., Jackson, K. E., and Lyle, K. H., "Finite Element Simulation of a Full-Scale Crash Test of a Composite Helicopter," *Journal of the American Helicopter Society*, Vol. 47, No. 3, July 2002, pp. 156–168. doi:10.4050/JAHS.47.156

[6] Fasanella, E. L., Boitnott, R. L., Lyle, K. H., and Jackson, K. E., "Full-Scale Crash Test and Simulation of a Composite Helicopter," *International Journal of Crashworthiness*, Vol. 6, No. 4, 2000, pp. 485–498.

Table 2 Summary of results

	Acceleration			Pressure P4			Pressure P1		
Impact velocity, m/s	Predicted, g	Measured, g	Error, %	Predicted, KPa	Measured, KPa	Error, %	Predicted, KPa	Measured, KPa	Error, %
3	15	12	+20	86	68	+20	58	86	−32
8	46	40	+13	250	195	+22	130	300	−56
10	56	46	+18	290	250	+13	190	340	−44

doi:10.1533/cras.2001.0192
[7] Fasanella, E. L., Jackson, K. E., Sparks, C. E., and Sareen, A. K., "Water Impact Test and Simulation of a Composite Energy Absorbing Fuselage Section," *Journal of the American Helicopter Society*, Vol. 50, 2005, Paper 150.
doi:10.4050/1.3092852
[8] Randhawa, H. S., and Lankarani, H. M., "Finite Element Analysis of Impacts on Water and its Application to Helicopter Water Landing And Occupant Safety," *International Journal of Crashworthiness*, Vol. 8, No. 2, Jan. 2003, pp. 189–200.
doi:10.1533/ijcr.2003.0229
[9] Hughes, K., Campbell, J., and Vignjevic, R., "Application of the Finite Element Method to Predict the Crashworthy Response of a Metallic Helicopter Under Floor Structure onto Water," *International Journal of Impact Engineering*, Vol. 35, No. 5, 2008, pp. 347–362.
doi:10.1016/j.ijimpeng.2007.03.009
[10] Pentecôte, N., and Vigliotti, A., "Crashworthiness of Helicopters on Water: Test and Simulation of a Full-Scale wg30 Impacting on Water," *International Journal of Crashworthiness*, Vol. 8, No. 6, Jan. 2003, pp. 559–572.
doi:10.1533/ijcr.2003.0259
[11] Hallquist, J. O., "Time Integration," *LS-DYNA Theory Manual*, Livermore Software Technology Corp., Livermore, CA, March 2006, Chap. 21.
[12] Hallquist, J. O., "EOS," *Keyword User's Manual, Version 971*, Livermore Software Technology Corp., Livermore, CA, March 2007, pp. 15.1–15.44.
[13] "Simulating Forces and Loads," *MSC.Patron User's Guide Version 2010*, MSC Software Corp., Santa Ana, CA, 2005, pp. 141–173.
[14] "The Create Action (FEM Entities)," *MSC.Patran Reference Manual Part 3: Finite Element Modeling, Version 2010*, MSC Software Corp., Santa Ana, CA, 2005, pp. 101–149.
[15] Hallquist, J. O., "Keyword File Editing," *LS-PrePost Manual, Version 1.0*, Livermore Software Technology Corp., Livermore, CA, 2002, pp. 85–113.
[16] Hallquist, J. O., "Pre Processing Tools," *LS-PrePost Manual, Version 1.0*, Livermore Software Technology Corp., Livermore, CA, 2002, pp. 113–150.
[17] Belytschko, T., Liu, W. K., and Moran, B., "One Point Quadrature Elements," *Non-Linear Finite Elements for Continua And Structures*, Wiley, New York, 2000, pp. 563–566.
[18] Belytschko, T., Lin, J., and Tsay, C. S., "Explicit Algorithms for Nonlinear Dynamics of Shells," *Computer Methods in Applied Mechanics and Engineering*, Vol. 42, No. 2, 1984, pp. 225–251.
doi:10.1016/0045-7825(84)90026-4
[19] Gingold, R. A., and Monaghan, J. J., "Smoothed Particle Hydrodynamic: Theory and Application to Non-Spherical Stars," *Monthly Notices of the Royal Astronomical Society*, Vol. 181, 1977, pp. 375–389.
[20] Cleary, P. W., and Monaghan, J. J., "Boundary Interactions and Transition to Turbulence for Standard CFD Problems," *SPH Proceedings of the 6th International Computational Techniques and Applications Conference*, Canberra, Australia, CSIRO, Sydney, Australia, 1993, pp. 157–165.
[21] Lacome, J. L., "Smoothed Particle Hydrodynamics (SPH): A New Feature in LS-DYNA," *Proceedings of the 6th International LS-DYNA Users Conference*, Dearborn, MI, 2002, pp. 29–34.
[22] Souli, M., and Benson, D. J., *Arbitrary Lagrangian-Eulerian and Fluid-Structure Interaction*, Wiley, New York, 2010.
[23] Stellingwerf, R. F., and Wingate, C. A., "Impact Modelling with Smooth Particle Hydrodynamics," *International Journal of Impact Engineering*, Vol. 14, Nos. 1–4, 1993, pp. 707–718.
[24] Gingold, R. A., and Monaghan, J. J., "Kernel Estimates as a Basis for General Particle Methods in Hydrodynamics," *Journal of Computational Physics*, Vol. 46, 1977, pp. 429–453.
doi:10.1016/0021-9991(82)90025-0
[25] Hertel, E., Jr., and Kerley, G., "Manual: The Equation of State Package," Sandia National Labs., TR SAND98-0947, Livermore, CA, 1998.
[26] "Recommended Practice: Instrumentation for Impact Test, Part 1," Soc. of Automotive Engineers Electronic Instrumentation TR J211/1, March 1995.
[27] Guida, M., Marulo, F., Meo, M., and Riccio, M., "Analysis of Bird Impact on a Composite Tailplane Leading Edge," *Applied Composite Materials*, Vol. 15, Nos. 4–6, 2008, pp. 241–257.
doi:10.1007/s10443-008-9070-6
[28] Guida, M., Marulo, F., Polito, T., Meo, M., and Riccio, M., "Design and Testing of a Fiber Metal Laminate Bird Strike Resistant Leading Edge," *Journal of Aircraft*, Vol. 46, No. 6, 2009, pp. 2121–2129.
doi:10.2514/1.43943
[29] Anghileri, M., Castelletti, L. M. L., and Tirelli, M., "Fluid–Structure Interaction of Water Filled Tanks During the Impact with the Ground," *International Journal of Impact Engineering*, Vol. 31, No. 3, 2005, pp. 235–254.
doi:10.1016/j.ijimpeng.2003.12.005